Large Eddy Simulations using High order Flux Reconstruction method on Hybrid Unstructured meshes

Yi Lu *
Whittle Lab, University of Cambridge, Cambridge, UK, CB3 0DY
Kai Liu †
Dept. Thermal Engineering, Tsinghua University. Beijing, China, 100084
W.N.Dawes‡
Whittle Lab, University of Cambridge, Cambridge, UK, CB3 0DY

Large eddy simulations using hybrid unstructured meshes are performed for different problems including external flows and internal flows. This code is based on a novel variant of high order flux reconstruction methods which is robust and efficient. Both implicit second order backward differentiation formula(BDF2) with nonlinear block LU-SGS as inner iterative and an explicit space-time method are implemented for unsteady time-marching. A prediction-correction type space-time method was introduced, which allows very efficient local time-stepping for unsteady simulations including LES. Time accuracy is ensured by the time-integration of correction flux under the space-time framework by using an extended continuous Runge-Kutta method. This method is smoothly combined with the high order flux-reconstruction discretization. The accuracy, efficiency and the potential to solve large-scale, real geometry problems of the new solver algorithm is demonstrated.

I. Introduction

Computational Fluid Dynamic(CFD) is widely used in different industry areas at present, while almost all commercial and government codes are based on algorithms developed more than 20 years ago, these codes are successfully to solve complex geometry problems with the support of turbulence modeling but are generally limited to 2nd order accuracy. With the increasing computational abilities, Large eddy simulations(LES) are more and more attractive for industry for its more general ability to handle turbulence without modeling. Whereas, there are still two bottlenecks which inhibit LES to solve realistic problems as the current production codes: one is the hybrid unstructured meshes are necessary to handling these geometries, the simulations with at most 2nd order accuracy on these meshes by using current production solvers limit their ability to correctly represent the whole energy spectrum resolved in LES, which indicate high order methods on unstructured grid have more advantages for high resolution LES; another challenge is the huge computational cost caused by not just high order space discretization requirements but also high accurate time resolution for vortex preserving. In this work, the local reconstruction, high order, differential form Flux Reconstruction(FR) method are implemented to support tetrahedrons, pyramids, prisms and hexahedrons up to fourth order, which can achieve very high efficient space discretization and is able to resolve turbulence using much coarser mesh than 2nd methods; in order to improve unsteady time marching efficiency, both implicit method and explicit method are adopted and tested, especially an efficient space-time extension of FR method is presented which allows local time-stepping for each cell in time-accurate simulations and is able to achieve arbitrary order along the time direction. Compared to traditional time discretizations using uniform timesteps, this extension overcome the small cell size limitation and makes the

*Research Associate, Whittle Lab, University of Cambridge, UK, and AIAA Associate Member.
†phD student, Thermal Engineering Department, Tsinghua University, China.
‡Professor, Whittle Lab, University of Cambridge, UK, and Senior AIAA Member.

computational cost of LES scalable, at least in principle, for any scale problem, especially for large scale and multi-scale problems within complex geometries. This new method has the potential to be significantly faster than conventional approaches for large-scale and multi-scale simulations. In the present work, the large eddy simulations for internal flows including low pressure turbine blade, low pressure turbine blade with endwall, and also periodic arrays of a single film-cooling hole ; for external flows, the wall-resolved LES for the low Reynolds number flow around a sphere, high Reynolds number flow around a sphere and high Reynolds number around high lift airfoil, are presented. Detail flow structures and comparison with experiment data for selected simulations are presented and discussed. There is no explicit sub-grid model implemented in this work which indicate all simulations are performed by implicit LES. The efficiency of the new solver algorithm is demonstrated.

II. Flux Reconstruction Discretization

This differential form FR method was firstly introduced by Huynh[1] for 1D problems and extended to quadrilaterals and hexahedrons by simple tensor-product. Wang and Gao[2] extended this method to simplex elements with the correction procedure via reconstruction method in 2009. Based on the same idea, Jameson et al[3][4] identified an infinite range of high-order energy stable flux reconstruction (FR) schemes on 1D elements, quadrilaterals, hexahedrons and 2D triangular elements. The FR method can be cast the same as discontinuous galerkin(DG) method mathematically and is proved nonlinearly stable for all elements if aliasing error can be damped.[5] Based on the previous implementation, special FR coefficients are developed to enhance the robustness for complex unstructured meshes[6] and adopted in this work.

In FR discretization, in order to deal with general unstructured meshes including high order curved

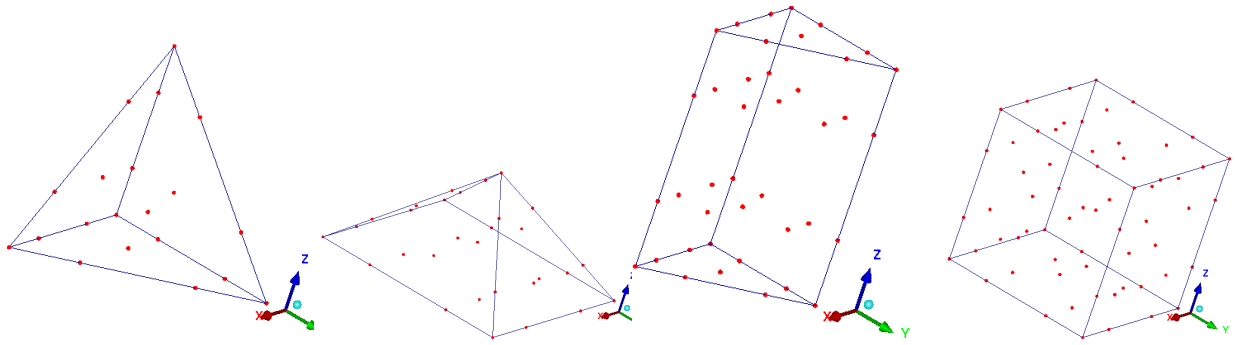

Fig 1. 4^{th} **order solution points for 3D Elements**

cells, all elements are transformed from the physical domain (x, y, z) to computational(local) domain (ξ, η, ζ). Following the coordinates transformation, define

$$\begin{aligned} \hat{U} &= |J|U \\ F^{\xi} &= |J|(\xi_x F^x + \xi_y F^y + \xi_z F^z) \\ F^{\eta} &= |J|(\eta_x F^x + \eta_y F^y + \eta_z F^z) \\ F^{\zeta} &= |J|(\zeta_x F^x + \zeta_y F^y + \zeta_z F^z) \end{aligned} \tag{1}$$

The Jacobian matrix J corresponding to the transformation takes the following form

$$J = \frac{\partial(x, y, z)}{\partial(\xi, \eta, \zeta)} = \begin{bmatrix} x_\xi & x_\eta & x_\zeta \\ y_\xi & y_\eta & y_\zeta \\ z_\xi & z_\eta & z_\zeta \end{bmatrix} \tag{2}$$

The governing equation of Navier-Stokes equation in computational(local) domain becomes

$$\frac{\partial \hat{U}}{\partial t} + \nabla^{\xi} \cdot \vec{F}^{\xi} = \frac{\partial \hat{U}}{\partial t} + \frac{\partial F^{\xi}}{\partial \xi} + \frac{\partial F^{\eta}}{\partial \eta} + \frac{\partial F^{\zeta}}{\partial \zeta} = 0 \tag{3}$$

figure 1 gives the 4th order solution points for different kinds of 3D elements including for the tetrahedrons, pyramids, prisms and hexahedrons which make up a general, hybrid unstructured meshes. For the j-th solution points of i-th element in a non-overlapped mesh, the uniform FR discretization for different types of elements are given as

$$\frac{\partial \hat{U}^h_{i,j}}{\partial t} + (\nabla^\xi \cdot \vec{F}^\xi(U^h_i))_{i,j} + \sum_{f=1}^{N_s}\sum_{l=1}^{K_f} \alpha_{j,f,l}(\widetilde{F}^\xi|_n - F^\xi|_n)_{i,f,l} = 0 \tag{4}$$

Where N_s is number of sides for the element and K_f equals number of flux points on the side, $\widetilde{F}^\xi$, $\widetilde{F}^\eta$ and $\widetilde{F}^\zeta$ denote the common flux which take the form of Riemann fluxes for the inviscid flux and central averaged values for viscous part, and α is flux reconstruction coefficients for standard element. Particularly, the difference between common flux and the outer normal projection of local flux $\widetilde{F}^\xi|_n - F^\xi|_n$ is called "correction flux" in FR method.

II..1. Implicit time-marching method

The implicit BDF2 implemented in this paper for unsteady simulations with LU-SGS for inner iteratives is given as

$$\left(\frac{I}{\Delta t_n} - \frac{3}{2}\frac{\partial R_i}{\partial U_i}\right)(U^{(k+1)} - U^*)_i = \frac{3}{2}R_i(U^*) + \frac{1}{3\Delta t_n}(U^n_i - U^{n-1}_i) - \frac{U^*_i - U^n_i}{\Delta t_n} \tag{5}$$

where $(\cdot)^k$ denotes the index of the inner iterations between $n-$th and $n+1-$th time steps and $(\cdot)^*$ denotes the most recent update the symmetric lower or upper sweeps over the global domain. In order to improve inner iterative efficiency, for boundary layer mesh with large aspect ratio cells, the gauss-seidel interatives are performed along the "elem line" perpendicular to boundary as the element indexes shown by figure 2.

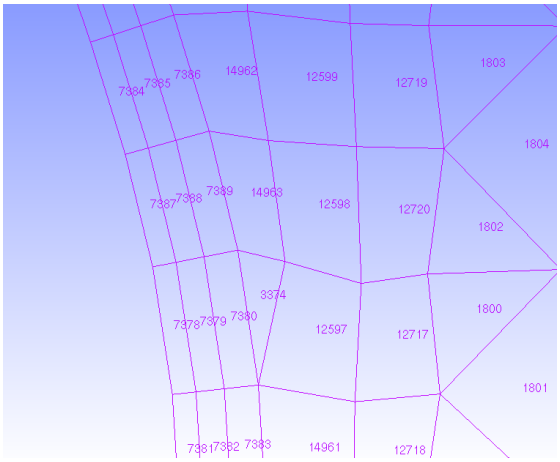

Figure 2. Line implicit reorder for boundary layer mesh

II..2. Explicit space-time expansion

For time-dependent ODE(ordinary differential equations), the so-called "space-time" type numerical method has great potential to achieve high order time accuracy and provide more flexibility for its discretization along time marching direction. So far, there are two types of space-time extension based on high order local reconstruction methods: one is the global space-time DG scheme developed by van der Vegt and van der Ven[7] for inviscid flow, and extended for compressible Navier-Stokes equations by Klaij et al[8]which results in a set of global nonlinear equations; the other one is based on predictor-corrector method-Gassner et al[9] reviewed different types of local predictors for DG and FVM, including Cauchy-Kowalevsky(CK) procedure[10]-,[13] continuous Galerkin predictor,[14] and a local continuous extension Runge-Kutta predictor.[15]

The space-time extension of high order FR schemes is introduced by the present authors in[16] and,[17] and results in a very efficient code with special parallel partition method with multi-constraints for load balancing

of the non-regular time marching process, and pure-asynchronous parallel massage passing interface(MPI) for the sake of high speed up ratio on clusters or many-core systems. Firstly rewrite Eq.(4) as

$$\frac{\partial U_{i,j}}{\partial t} = \mathbb{R}^D_{i,j}(U_i) + \sum_f^{N_f} \mathbb{R}^C_{i,j,f}(U_i, U^{nb}_{i,f}) \tag{6}$$

where

$$\mathbb{R}^D_{i,j}(U_i) = -\frac{1}{|J|_{i,j}}(\nabla^\xi \cdot \vec{F}^\xi(U^h_i)_{i,j} \tag{7}$$

$$\mathbb{R}^C_{i,j,f}(U_i, U^{nb}_{i,f}) = -\frac{1}{|J|_{i,j}} \sum_{l=1}^{K_f} \alpha_{j,f,l}(\widetilde{F}^\xi|_n - F^\xi|_n)_{i,f,l} \tag{8}$$

For Eq.(6), start a simple integration in time of the semi-discrete formulation for j-th solution point in i-th element from time level t_n to time level t_{n+1}

$$U^{n+1}_{i,j} - U^n_{i,j} = \int_{t_n}^{t_{n+1}} \mathbb{R}^D_{i,j}(U_i) + \sum_f^{N_f} \mathbb{R}^C_{i,j,f}(U_i, U^{nb}_{i,f}) dt \tag{9}$$

Eq.(7) indicates $\mathbb{R}^D$ is the flux divergence which is completely local for each element, while $\mathbb{R}^C$ is linear combination of "correction flux" used to update the DOFs of local element, split the right hand side of (9) by using $\mathbb{R}^D$ as a predictor and the time integration of $\mathbb{R}^C$ as a corrector along time direction. This leads to our space time expansion flux reconstruction method(STEFR) as

$$U^{n+1}_{i,j} = v^{n+1}_{i,j} + \int_0^{\Delta\tau} \sum_f^{N_f} \mathbb{R}^C_{i,j,f}(v_i(\tau), v^{nb}_{i,f}(\tau)) d\tau \tag{10}$$

while $\Delta\tau = t^{n+1} - t^n$, the space-time polynomial $v(\tau)$ is computed by a local predictor, in this work the continuous extension Runge-Kutta method[18] is adopted as

$$\begin{aligned} v_{i,j}(\tau) &= U^n_{i,j} + \Delta\tau * \sum_{l=1}^{N_{stages}} b_l(\tau) k_l \\ b_l(\tau) &= \sum_{m=1}^{O_t} \mathbf{b}_{l,m} * \tau^m \\ k_l &= \mathbb{R}^D_{i,j}(v_l) \\ v_l &= U^n_{i,j} + \Delta\tau * \sum_{n=1}^{l} \mathbf{a}_{l,n} k_{l-1} \end{aligned} \tag{11}$$

where O_t is the order of time discretization and N_{stages} is related number of stages, the coefficients $\mathbf{b}$ and $\mathbf{a}$ are given by.[18]

From the above development, it can be seen that the predictor procedure is completely local for every element and the correction is only relies on time integration of correction fluxes, which implies the local time step can be implement for time accurate simulations, and the conservation of both space and time is ensured by one-side time integration of the "correction flux" as Eq.(10).

In actual implement, each cell has a integer index named "time tree" which records the physical time and is updated only after correction. The model evolution with 3 elements is shown in figure 3, where the middle red element use half time steps compared to the two blue elements and it has priority to implement its correction by using the predicted DOFs of its neighbors. Corrections of the two blue elements will be delayed until matched by the time integration of correction flux computed by the red element. The controlling of this local time stepping process is cumbersome and very difficult, but very efficient once achieved because the computational cost is not dependent on the smallest cell, and it is able to achieve arbitrary order for time also. The history of the "time-tree" of all elements over one global time step for a real test case is shown in figure 4.

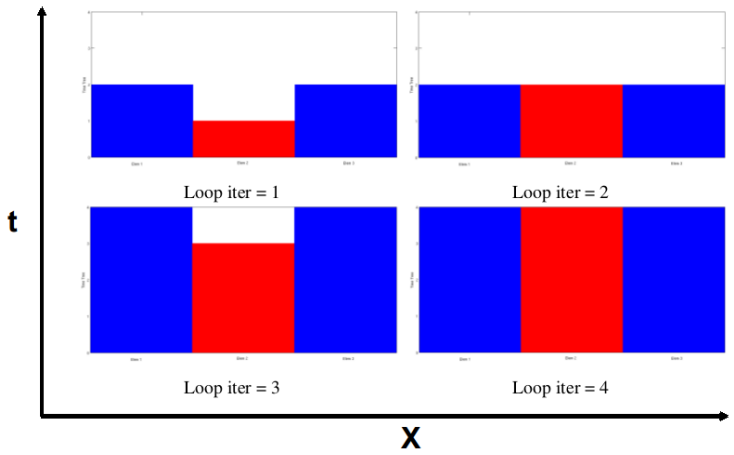

Figure 3. Sequence of steps of a model evoluation with 3 elements and local time stepping advancing to a new global time

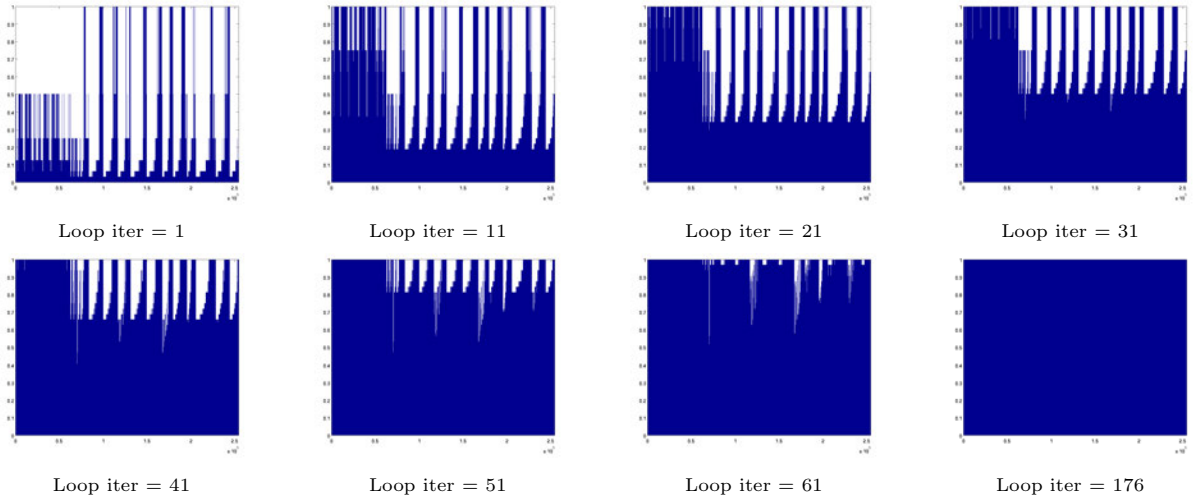

Figure 4. Snapshots of transient "time-tree" during one time-step: horizontal is element index and vertical is normalized time tree.

III. Numerical Simulations and Analysis

All meshes used in this paper were generated by an state-of-art mesh generation system, BOXERMesh.[20]

III.A. Low Pressure Turbine blade

This testcase concerns the LES of the transitional and separated flow on the T106C high-lift subsonic turbine cascade. The Reynolds number of 80.000 chosen for this work. As the inlet turbulence is very low (turbulence intensity of 0.9%), the flow features laminar separation and a relatively slow natural transition. Blade pressure distribution and wake total pressure loss profiles have been measured at the von Karman institute (VKI) in the closed loop tunnel.[19] The conditions are derived in A, and are summarized as:

- inlet total pressure: $p_t = 7189.5Pa$;
- inlet total temperature: $T_t = 298.15K$;
- pitchwise inlet flow angle 32.7° from the axial direction;
- the exit static pressure $p_b = 5419.3Pa$;

The spanwise extention of the blade is $S = 0.2C$, where C is the length of axial chord. Two kinds of

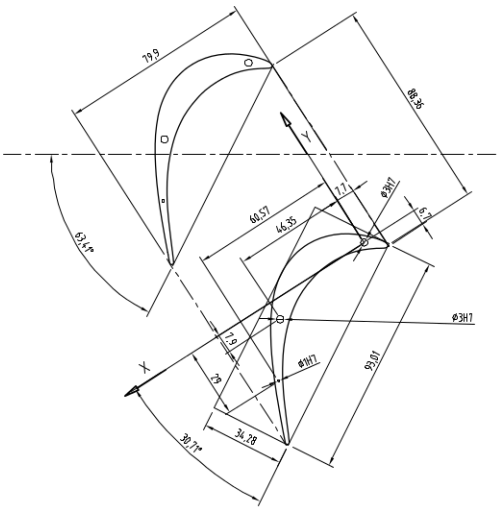

a.Geometrical description of the blade section (Courtesy VKI)

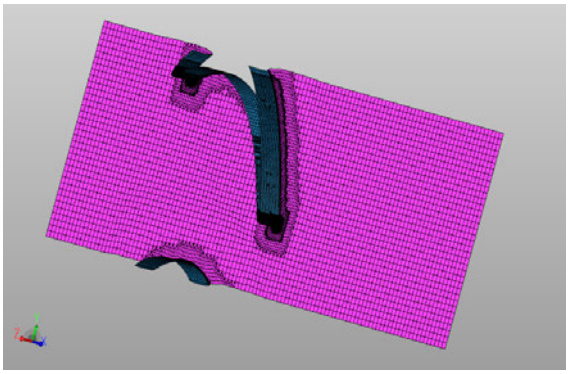

b. Fine mesh for second order simulation

Figure 5. Geometry and mesh snapshot

mesh are used for this work: 3D meshes extruded along spanwise from a 2D mesh slices around the blade, and the full 3D hybrid unstructured meshes. All configurations and computational cost statistics for these four simulations are given in table 1. An high order mesh generation method based on local high order reconstruction are developed which is able to handle general unstructured meshes, the comparison of outer normal of blade surface between original first order mesh and third order mesh after high order modification are presented by figure 6.

Table 1. Simulation configurations and computational cost

Order&Mesh	nCells	nDofs	y^+	dt	Time(h) for 1 T_p	Riemann Flux	Max E_{inner}
2^{nd}&Extrude	3×10^6	1.15×10^8	< 1	1×10^{-7}	15.4	HLLC	10^{-4}
2^{nd}&Hybrid	2×10^6	7.3×10^7	< 1	1×10^{-7}	16.2	HLLC	10^{-4}
3^{rd}&Extrude	3.5×10^5	4.5×10^7	< 1.3	1×10^{-7}	17.5	HLLC	10^{-4}
3^{rd}&Hybrid	5.1×10^5	5.8×10^7	< 1.3	1×10^{-7}	16.5	Rusanov	10^{-4}

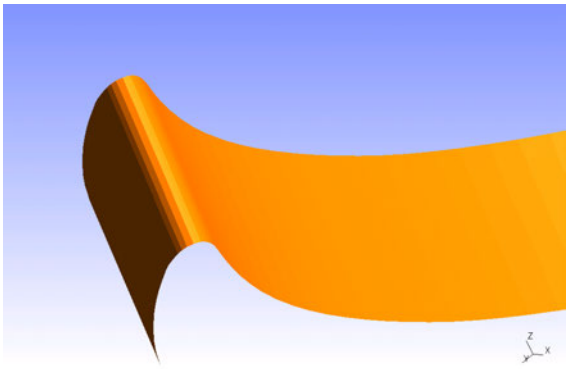

a. Original first order mesh

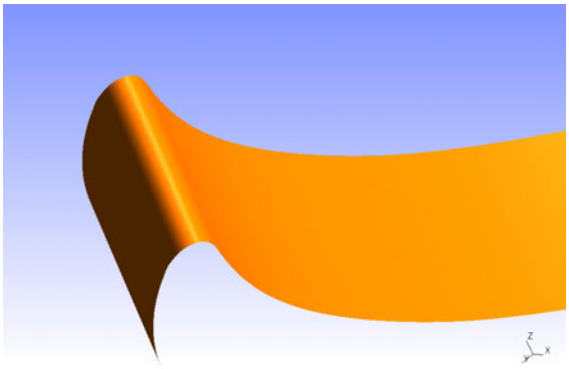

b. Third order mesh

Figure 6. Outer normal of blade surface

The time maching method used for this case is BDF2 with BLU-SGS as inner iteratives, and all maximum relative inner iterative error are lower than 1×10^{-4} to assure the time accuracy. All simulations are performed on 8CPUs&128 cores(Intel 9600 2.60GHz Sandy Bridge).

Figure 7 show the transient iso-surface of Q-criterion for the simulation using third order with extruded

mesh, and the time-averaged pressure distribution for the simulation using third order with hybrid unstructured mesh. The time-averaged ISO mach number is given by figure 8(a) and compared with experiment data, from the discussion at 2nd International Workshop on High-Order CFD Methods,[21] there maybe some unmatched inlet flow angle of the simulation and real experiments which cause deviation of the results especially at the turbulent region. However, the total pressure in the wake region given by figure 8(b) still indicate that third order simulations have less numerical dissipation even with much less cells.

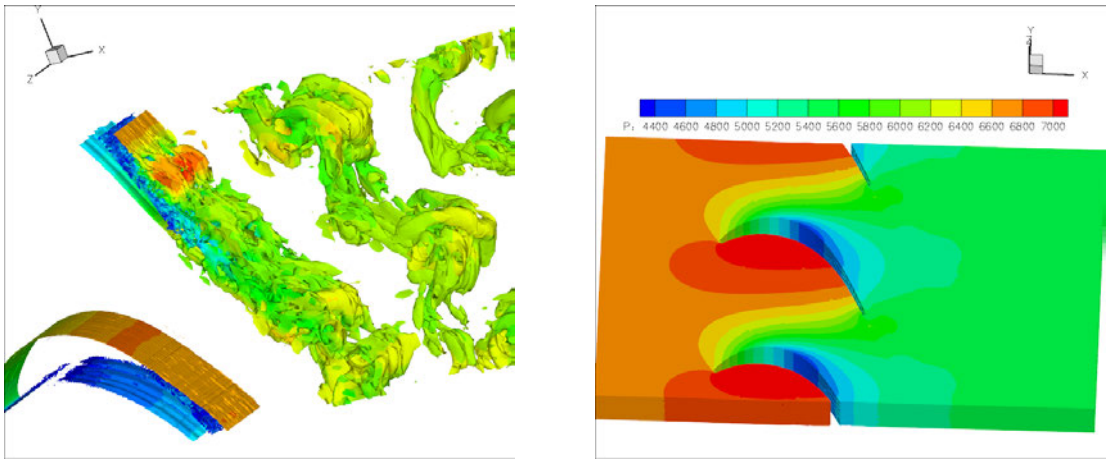

a.Snapshot of transient Q-criterion for 3^{rd}&Extrude simulation

b. Time-averaged pressure distribution for 3^{rd}&hybrid simulation

Figure 7. Low pressure turbine blade result

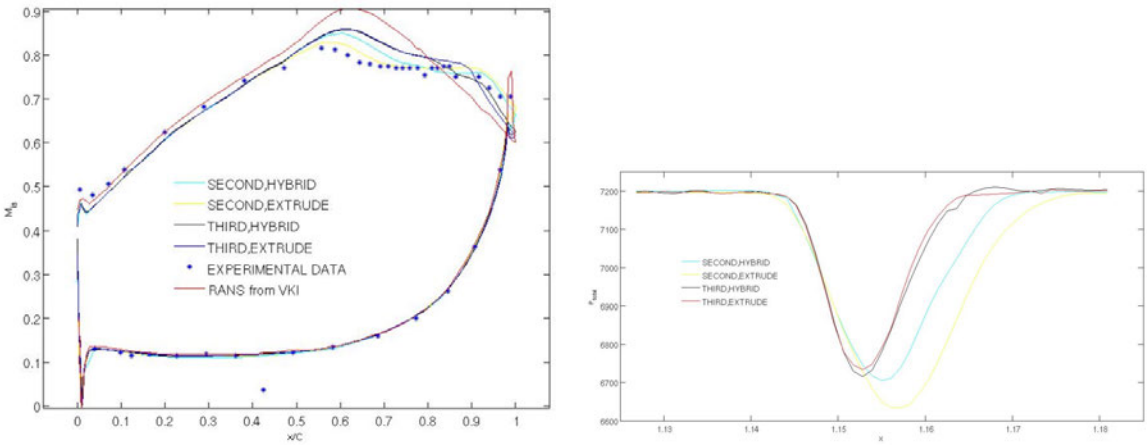

a.Time-Average ISO Mach number

b. Total pressure in the wake region

Figure 8. Mean flow coefficients and the comparison with experiment data

III.B. Low-Re/High-Re flow around sphere

The low Reynolds number(Re=300) flow and high Reynolds number(Re=10000) flow around sphere are simulated using hybrid unstructured meshes as figure 9 shown. The Iso-surface of Q criterion for different simulations are given in figure 10 which indicate higher order simulation have better resolution for vortex region. The drag coefficient C_d and Strouhal number S_t are listed in table 2 with the comparisons with other calculations and experiments. The space-time method was adopted for this case for unsteady time marching.

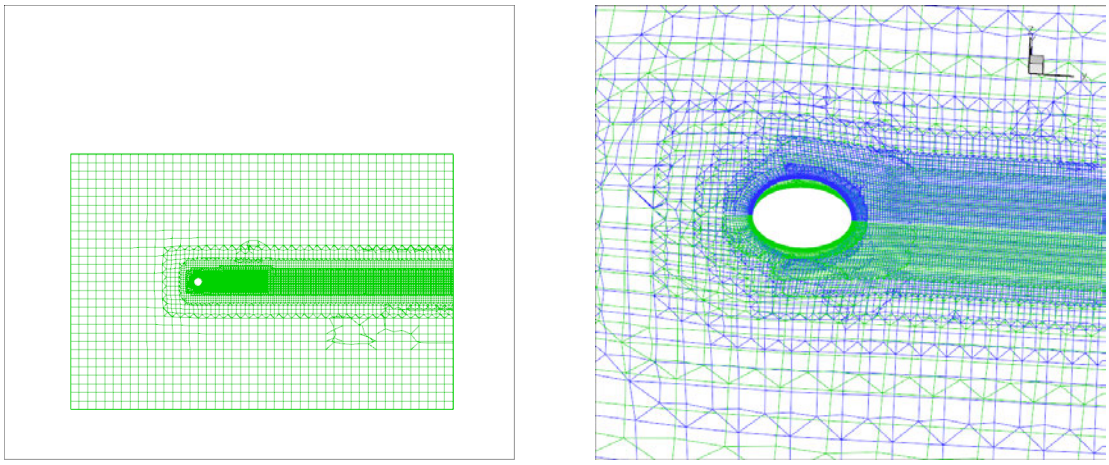

a.Slice of computational domain b. Mesh

Figure 9. Computational domain and mesh slice

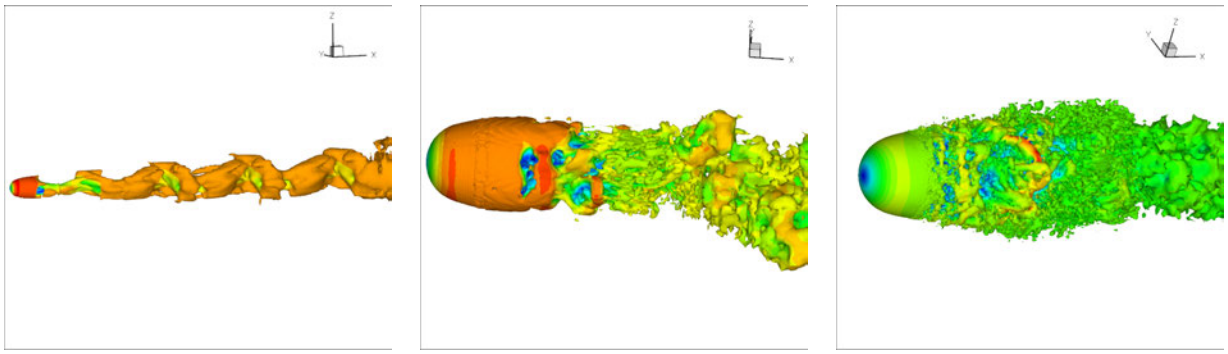

a.Re=300,SECOND b.Re=10000, SECOND b.Re=10000, THIRD

Figure 10. Snapshot of transient ISO-Surface of Q criterion (Q=-100000)

III.C. Film-cooling hole

The geometry configurations for three different type of cooling holes are given by figure11(a). Also figure11(b) (d) shows the 3D models of each hole, $D = 4mm$ is the diameter for all three holes. All geometries and configurations are obtained from previous work.[18]

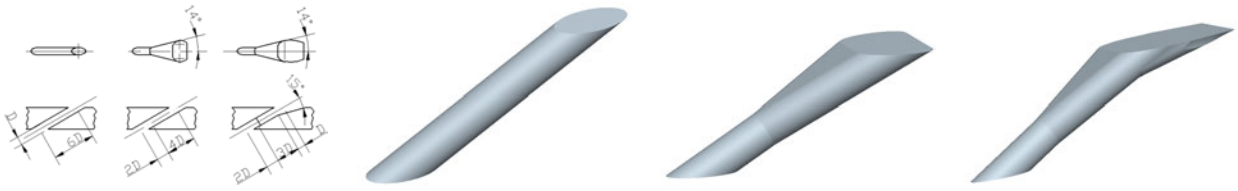

a. Geometry configurations b. Cylindrical hole c. Fan Shaped hole d. Fan Shaped hole with Laid-Back

Figure 11. Cooling Hole

Table 2. Result of Low-Re/High-Re flow around a sphere

Re	Order	nCells	C_d	C_d (calc/expt)	S_t	S_t (calc/expt)
300	SECOND	401839	0.681	0.656	0.1347	0.134
				0.657		0.136
				0.658		0.136
				0.671		0.137
10000	SECOND	1062089	0.443	0.393		$0.195S_{t1}$
				0.438		$0.181S_{t1}$
				0.40 ± 0.01		$1.30\text{-}1.85S_{t2}$
10000	THIRD	519747	0.4429	0.393		$0.195S_{t1}$
				0.438	$0.1879S_{t1}$	$0.181S_{t1}$
				0.40 ± 0.01	$0.128S_{t2}$	$1.30\text{-}1.85S_{t2}$

The flow conditions for the mainstream are given by table 3, and the Reynolds number based on mainstream flow and the pitchwise hole spacing is $Re = 1.8 \times 10^4$. This is typical of cooled blade platform conditions. The blowing ratio MFR is defined as:

$$MFR = \frac{\rho_c U_c}{\rho_\infty U_\infty} \tag{12}$$

Table 3. Flow parameters of mainstream

Ma_∞	$U\infty$(m/s)	Tu_∞(%)	T_∞(K)	P_∞(Pa)
0.047	16	5.0	288	99600

where $(\cdot)_c$ are flow parameters for the cooling holes given by table 4.

Table 4. Flow parameters of cooling holes

Run ID	Hole type	MFR	T_c(K)	N_{cells}
1	Cylindrical	0.5	273	1.09M
2	Cylindrical	1.0	273	1.09M
3	Cylindrical	1.5	273	1.09M
4	Fan Shaped	0.5	273	1.32M
5	Fan Shaped	1.0	273	1.32M
6	Fan Shaped	1.5	273	1.32M
7	Laid-Back Fan Shaped	0.5	273	1.43M
8	Laid-Back Fan Shaped	1.0	273	1.43M
9	Laid-Back Fan Shaped	1.5	273	1.43M

The computational domain is shown in figure12(a). The single inclined hole with pitchwise periodic boundaries is placed between mainstream and the plenum with coolant flow comes from the pipe. The unstructured meshes are generated by BOXERMesh. Local refinements were imposed inside of the cooling hole and the downstream of coolant jets as shown in and figure12(b). Appropriate layer meshes were included to support the near-wall flows, with $y(+) < 1$ enforced for the first boundary layer cells. Due to the local reconstruction FR approach, at least second order is achieved for general unstructured meshes in this work which is a distinct advantages for LES.

All simulations were performed on 16 Intel-Sandybridge CPUs and each CPU has 16 physical computational cores which is organized by OpenMP for higher efficiency of the space-time framework. A special pure-asynchronous parallel massage passing interface(MPI) was developed for communication between different CPUs. The physical time scale $T_c = D/u_\infty$ equals to 0.00025 seconds and consumes about 1.25 hours

on this 16×16 core resource for cylindrical cases.

Speed up ratios(SPRs) of the current space time code compared to a standard 2 stage continuous Runge-Kutta explicit time marching method are presented in table 5. It can be seen even for such simple geometries, the speed up ratio achieved is higher than 20 due the very strict global minimum time step which is scaled by Δx_{min}^2, where Δx_{min} is minimum element size commonly inside the boundary layer mesh. For a geometry with a larger scale range, like the blade itself fully cooled, the speed up ratio could be much larger-of order hundreds. Octree-based meshes are especially suited to the efficiency of the space-time technique.

Table 5. LES speed up ratios(SPR)

Run ID	1	2	3	4	5	6	7	8	9
SPR	26.64	26.64	26.64	21.4	21.4	21.4	24.12	24.12	24.12

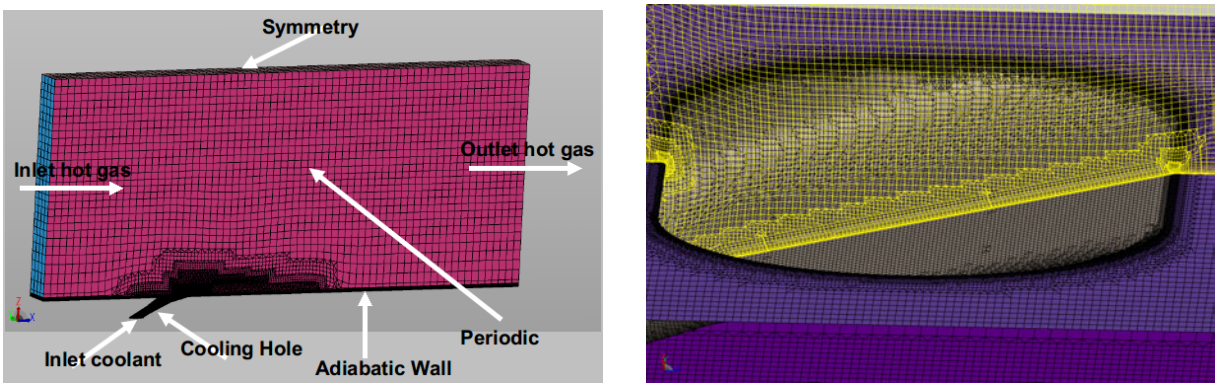

a. Computational domain b. Boundary layer mesh inside of cooling hole

Figure 12. Computational domain and ISO-Surface of mesh for Laid-Back Fan-Shaped cooling hole

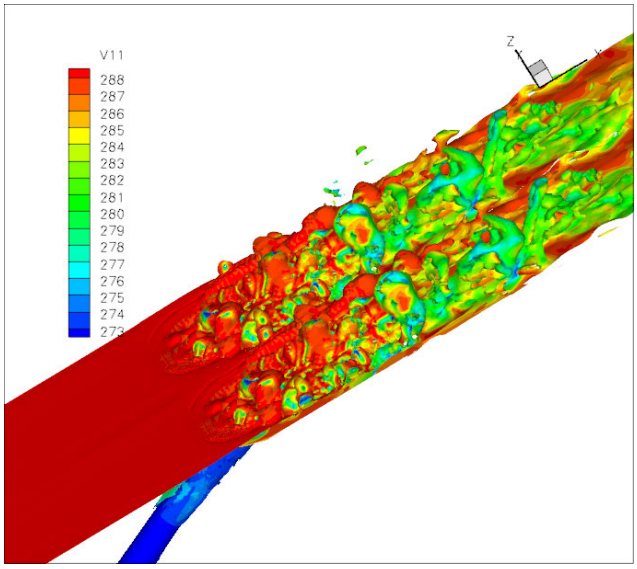

Figure 13. Vorticity magnititude for Fan Shaped hole with $MFR = 1.5$

III.D. Film cooling effectiveness

The film cooling effectiveness η is defined as

$$\eta = \frac{T_w - T_\infty}{T_c - T_\infty} \tag{13}$$

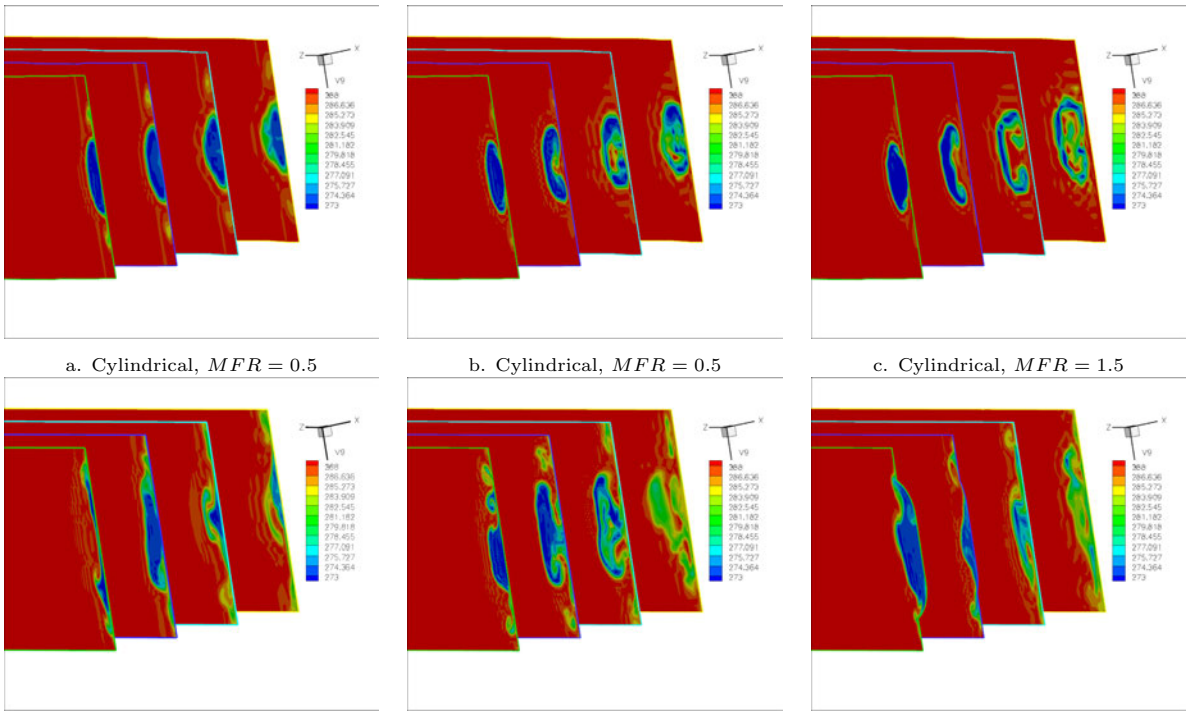

a. Cylindrical, $MFR = 0.5$ b. Cylindrical, $MFR = 0.5$ c. Cylindrical, $MFR = 1.5$

b. Fan Shaped, $MFR = 0.5$ e. Fan Shaped, $MFR = 1.0$ f. Laid-Back Fan Shaped, $MFR = 0.5$

Figure 14. Vortex structures in cross flow planes, coloured with temperature

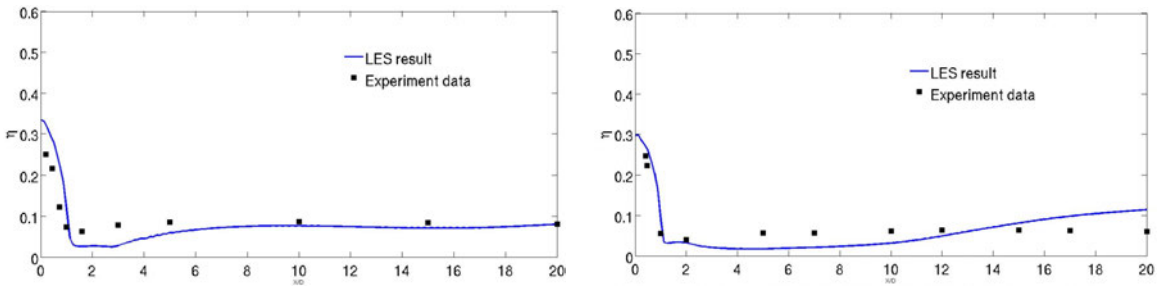

a. Cylindrical, $MFR = 1.0$ b. Cylindrical, $MFR = 1.5$

Figure 15. Time-averged, lateral averaged film cooling effectiveness and the comparison with experiment data

III.E. High Reynolds number airfoil flow

This case of the application of LES on an Aerospatial A-Airfoil at an angle of attack of 13.3° and $Re = 2.1 \times 10^6$, which is introduced by a project named LESFOIL,[23] and special enphasis is put on transition and separation. The computational domain is given by figure 16(a). There are two simulations performed in this work: one adopted traditional p-enrichment at the suction side, trailing edge and wake regions as shown in figure 16(b), where the transition and separation occur and develop; in another simulation, the enrichment was instead of higher order polynomial(third order) while most cells are still second order as the same as p-enrichment simulation. Detail computational configurations are listed in table 6. The spanwise extension is $0.03C$ where C is the length of chord.

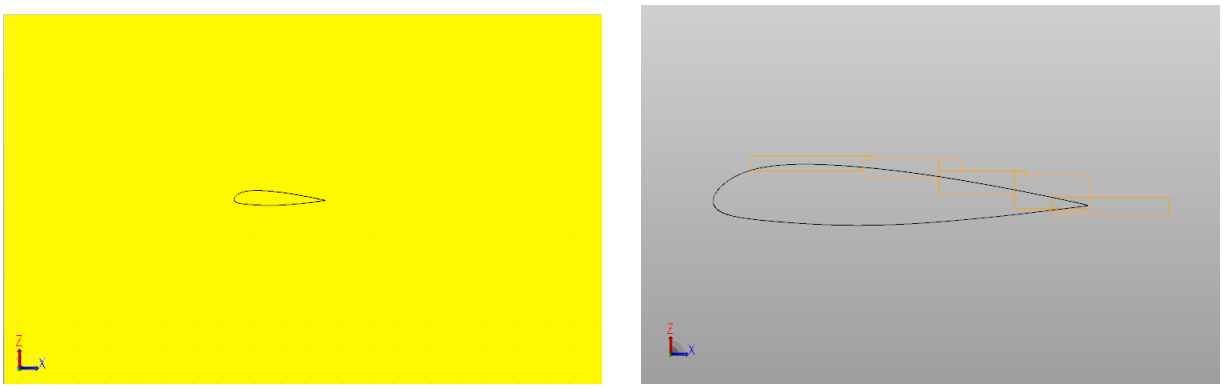

a. Computational domain b. p/h-enrichment region

Figure 16. Computational domain and p/h-enrichment for LESFoil

Table 6. Computational configurations of LESFoil case

Run ID	nCells	y^+	x^+	z^+	SPR	Time(h) for 1 Tp	Computational Resource
h-enrichment	2424060	1.3	108.3	108.3	14.4673	50	16CPU×16cores
p-enrichment	1771743	1.3	108.3	108.3	14.6943	57	32CPU×16cores

It should be notice that the x^+ and z^+ are only refer to the suction side and trailing edge including turbulent region, where the y^+ limitation for first boundary layer mesh is enforced for the whole areafoil surface. All simulations are performed using Intel-Sandybridge CPUs as the same as lowe pressure turbine blade case and film cooling case. Some results can be found in figure 17 figure 19.

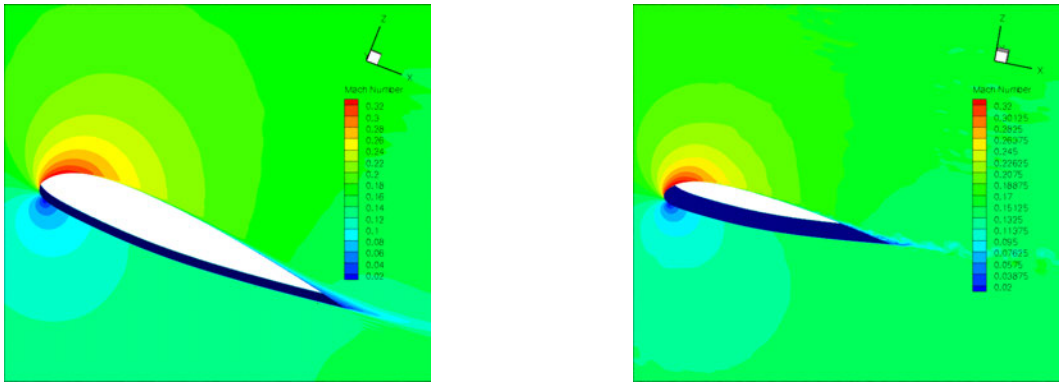

a. Time averaged Mach number snapshot b. Instantaneous Mach Number snapshot

Figure 17. Comparsion between mean flowfield and transient flowfield

III.F. Real geometry ship case

The number of cells for this ship with a landing helicoptor is around 73 millions, and the second order was used for the simulation with the number of total degree of freedoms(DOFs) is over 2 billions. The very low

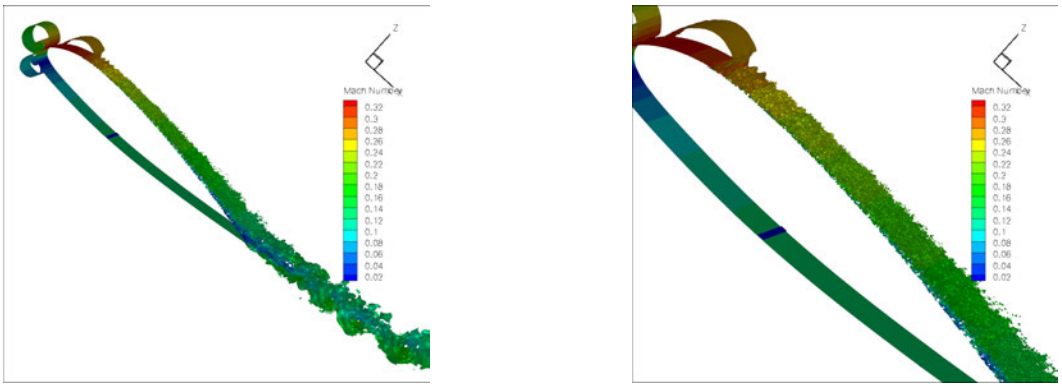

Figure 18. Q-criterion: Q = -10000, 10000, 1000000

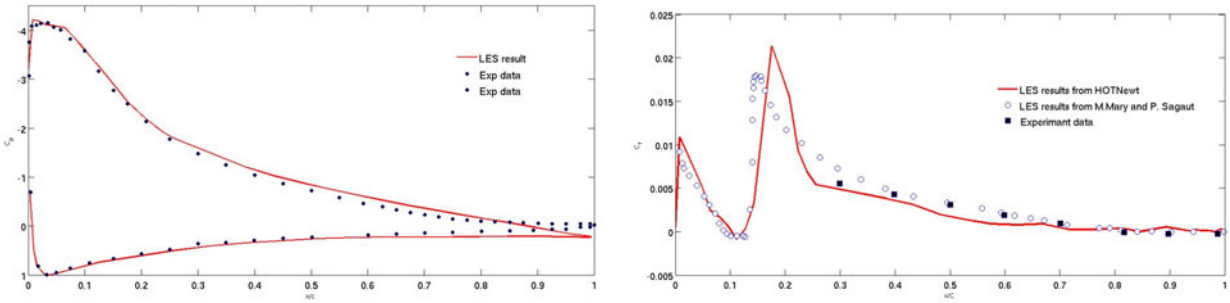

a. Mean pressure coefficients

a. Mean skin-friction coefficients

Figure 19. Comparsion between time-averaged results and experiment data

mainstream flow velocity is $7m/s$. Slip wall boundary condition was enfored for all surfaces of the helicoptor in order to simplify the simulation. This case is quite large scale with the length of the whole ship is over 140 meters, while the very small parts of radar antenna is resolved as shown in figure 20, the total time levels is 17 which means the ratio of timestep is $\Delta t_{max}/\Delta t_{min} = 2^{17} = 65536$. The simulation was implemented by 64 Intel-Sandybridge CPUs with 16 cores each, and only about 12 hours are needed to solve one flow passing time(mainstream flow pass the ship). Because of the very large geometry scale, the speed up ratio for this case achieved around 115 compared to second order Runge-Kutta time marching with uniform timestep. The statistics details of time levels is listed in table 7, and the iso-surface of mach number is shown in figure **??**.

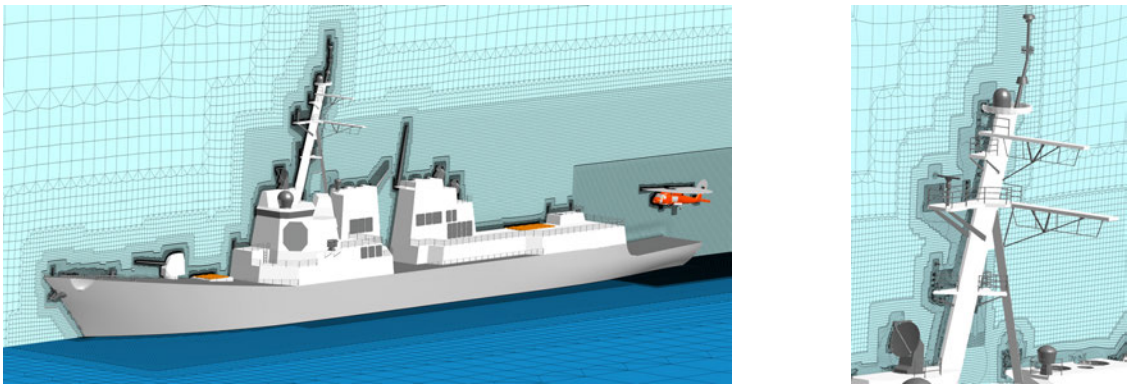

Figure 20. Mesh slice of a real geometry ship.

Tab 7. Statistics of time levels

N_{levels}	0	1	2	3	4	5	6	7	8
$\frac{\Delta t}{\Delta t_{max}}$	1.54e-5	3.1e-5	6.1e-5	1.2e-4	2.4e-4	4.8e-4	9.8e-4	2.0e-3	4.0e-2
N_{cells}	6	57	622	7.5e3	3.6e5	7.9e6	1.3e7	1.5e7	1.8e7
$\frac{N_{cells}}{N_{total}}$	8.2e-8	7.8e-7	8.5e-6	1.0e-4	0.5e-2	0.11	0.18	0.2	0.25

N_{levels}	9	10	11	12	13	14	15	16
$\frac{\Delta t}{\Delta t_{max}}$	7.8e-3	1.6e-2	0.03125	0.0625	0.125	0.25	0.5	1
N_{cells}	8.4e6	7.6e6	2.4e6	3.8e5	1.1e5	40324	17756	9020
$\frac{N_{cells}}{N_{total}}$	0.12	0.1	0.03	0.005	0.015	0.005	2.4e-4	1.2e-4

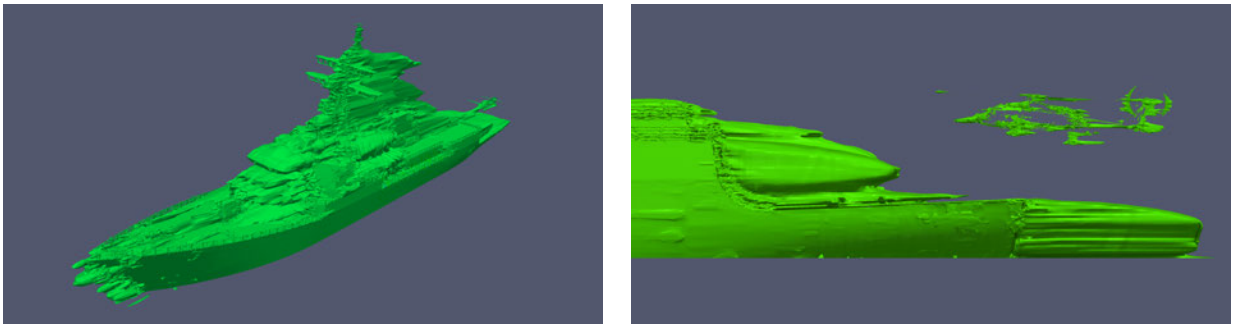

Figure 21. Iso-surface of mach number

IV. Conclusion

This paper has introduced a very efficient LES algorithm based on high order Flux Reconstruction combined with space-time integration and implementation on general, hybrid, unstructured meshes. Simulations of different flow problems demonstrated this new solver and displayed a wide range of interesting flow physics. The future work will try to solve large-scale, multi-scale problems with real geometries, and the study of efficient and robust sub-grid scale model and its coordinates with this algorithm will be investigated also.

Acknowledgments

This work is supported by Cambridge Flow Solutions Ltd. Thanks very much to Antonio d'Ammaro for helping to generate geometries for the film-cooling case and LESFoil case.

References

[1]H. T. Huynh A Flux Reconstruction Approach to High-Order Schemes Including Discontinuous Galerkin Methods*AIAA 2007-4079*

[2]Haiyang Gao, Z.J. Wang, Yen Liu, A Study of Curved Boundary Representations for 2D High Order Euler Solvers. *J Sci Comput.* (2010) 44: 323336

[3]Patrice Castonguay, Peter Vincent, Antony Jameson, Application of High-Order Energy Stable Flux Reconstruction Schemes to the Euler Equations, 2011

[4]A. Jameson, P.E. Vincent, P. Castonguay, On the Non-linear Stability of Flux Reconstruction Schemes, J Sci Comput, DOI 10.1007/s10915-011-9490-6

[5]A. Jameson, A Proof of the Stability of the Spectral Difference Method for All Orders of Accuracy, J. Sci. Comput., DOI 10.1007/s10915-009-9339-4 2009

[6]Yi Lu, Local Reconstruction High Order Method and Experimental Research for Internal Flow of Turbomachinery, PhD thesis, 2012.

[7]J. J. W. van der Vegt, H. van der Ven, SpaceTime Discontinuous Galerkin Finite Element Method with Dynamic Grid Motion for Inviscid Compressible Flows, I. General Formulation. Journal of Computational Physics 182(2002) 546585

[8]C.M. Klaij, J.J.W. van der Vegt, H. van der Ven, Spacetime discontinuous Galerkin method for the compressible Navier-Stokes equations.

[9]Gregor Gassner, Michael Dumbser, Florian Hindenlang, Claus-Dieter Munz. Explicit one-step time discretization for discontinuous Galerkin and finite volume schemes based on local predictors. Journal of Computational Physics 230(2011) 4232-4247

[10]J. Qiu, M. Dumbser, C-W Shu, The discontinuous Galerkin method with Lax-Wendroff type time discretizations, Comput. Methods Appl, Mech. Eng. 194(2005) 4258-4543

[11]A. Harten, B. Engquist, S. Osher, S. Chakravarthy, Uniformly high order essentially non-oscillatory schemes, III, J. Comput. Phys. 71 (1987) 23 1303.

[12]M. Dumbser, C.D. Munz, Building blocks for arbitrary high order discontinuous Galerkin schemes, J. Sci. Comput. 27 (2006) 215230.

[13]V.A. Titarev, E.F. Toro, ADER: arbitrary high order Godunov approach, J. Sci. Comput. 17 (14) (2002) 609618.

[14]V.A. Titarev, E.F. Toro, ADER schemes for three-dimensional nonlinear hyperbolic systems, J. Comput. Phys. 204 (2005) 715736.

[15]E.F. Toro, V.A. Titarev, Derivative Riemann solvers for systems of conservation laws and ADER methods, J. Comput. Phys. 212 (2006) 150165.

[16]M. Dumbser, D.S. Blasara, E.F.Toro, C.-D.Munz, A unified framework for the construction of one-step finite-volume and discontinuous Galerkin schemes on unstructured mehses. J.Comput.Phys. 227(2008) 8209-8253

[17]G. Gassner, F. Hindenlang, C.-D. Munz, A Runge-Kutta based Discontinuous Galerkin Method with Time Accurate Local Time Stepping. SimTech

[18]B. Owren, M. Zennaro, Derivative of efficient continuous explicit Runge-Kutta methods. SIAM, J.Sci.Stat. Comput. 13(1992) 1488-1501

[19]Jan Mich lek, Michelangelo Monaldi,Tony Arts, Aerodynamic Performance a of a Very High Lift Low Pressure Turbine Airfoil (T106C) at Low Reynolds and High Mach Number With Effect of Free Stream Turbulence Intensity, ASME Journal of Turbomachinery, volume 134, november 2012

[20]http://www.cambridgeflowsolutions.com/

[21]http://www.dlr.de/as/desktopdefault.aspx/tabid-8170/13999_read-35550/

[22]Jia Li&Yi Lu, Xin Yuan, Hongde Jiang. The measurement of Shaped Hole Film Cooling using Pressure Sensitive Paint. Journal of Tsinghua University(Science and Technology) 2010 Vol 08.

[23]Dahlstrom S. Davison L.(2000): Large Eddy Simulation of the Flow Around An Aerospatial A-aerofoil. ECCOMAS 2000, European Congress on Computational Methods in Applied Science and Engineering, 11-14 September, Barcelona, Spain.

[24]Jeong, J and Hussain, F., On the identification of a vortex, J. Fluid. Mech., 285, 69-94 (1995).

[25]Constantinescu, G.S., Chapelet, M.C. and Squires, K.D., Prediction of Turbulent Flow over a Sphere, AIAA Journal, 41, 1733-1742 (2003).

[26]Kim, J., Kim, D. and Choi, H., An Immersed-Boundary Finite-Volume Method for Simulations of Flow in Complex Geometries, Journal of Computational Physics, 171, 132 150 (2001).

[27]Giacobello, M., Wake structure of a transversely rotating sphere at moderate Reynolds numbers, Ph.D. thesis, The University of Melbourne, Department of Mechanical Engineering, September 2005.

[28]Tomboulides, A.G., Orszag, S.A. and Karniadakis, G.E., Direct and Large eddy simulations of axisymmetric wakes, AIAA paper number 93-0546, 1993.

[29]Taneda, S., Visual observations of the flow past a sphere at Reynolds numbers between 104 and 106, J. Fluid Mech., 85, 187-192, 1978.

[30]Kim, S.E., Large Eddy Simulation Using Unstructured Meshes and Dynamic Subgrid-Scale Turbulence Models, 34th AIAA Fluid Dynamics Conference and Exhibit, Portland, Oregon, AIAA paper number 2004-2548, 2004.

[31]Achenbach, E., Vortex shedding from spheres, J. Fluid Mech., 62, pp. 209-221, 1974.